Petroleum Science 23 (2026) 2821–2832

Contents lists available at ScienceDirect

Petroleum Science

journal homepage: www.keaipublishing.com/en/journals/petroleum-science

Original Paper

Potential application of hydrophobically modified Welan gum as a novel thermo-salt tolerant EOR agent in high-temperature and high-salinity reservoirs

Jia Chen [a,b], Zhao-Kai Wang [a,b], Wan-Lei Geng [a,b], Hao-Ran Cheng [c,d,*], Guang Zhao [a,b,**]

[a] School of Petroleum Engineering, China University of Petroleum (East China), Qingdao, 266580, Shandong, China
[b] State Key Laboratory of Deep Oil and Gas, China University of Petroleum (East China), Qingdao, 266580, Shandong, China
[c] School of Chemical Engineering, Qingdao University of Science and Technology, Qingdao, 266042, Shandong, China
[d] Sichuan Energy Internet Research Institute Tsinghua University, Chengdu, 610218, Sichuan, China

ARTICLE INFO

Article history:
Received 29 April 2025
Received in revised form
29 December 2025
Accepted 30 December 2025
Available online 2 January 2026

Edited by Yan-Hua Sun

Keywords:
Hydrophobically modified biopolymer
Welan gum
Hydrophobic association
Temperature and salt resistance
Enhanced oil recovery

ABSTRACT

Conventional polymeric systems face significant challenges in maintaining performance under high-temperature, high-salinity reservoir conditions due to limited thermal and saline stability. To address this critical limitation, a hydrophobically modified biopolymer (HWLG) was synthesized via etherification of Welan gum (WLG) with 1-bromooctadecane, introducing alkyl grafts to create hydrophobic microdomains. Comprehensive structural characterization was performed using Fourier transform infrared spectroscopy (FT-IR), nuclear magnetic resonance spectroscopy (NMR), gel permeation chromatography (GPC), thermogravimetry analysis (TGA), and scanning electron microscopy (SEM), confirming successful alkyl incorporation. Rheological evaluations demonstrated HWLG's concentration-dependent pseudoplasticity, achieving a viscosity of 1423.2 mPa·s at 4000 mg·L^{-1}, which was about 3.4 times that of WLG at 70 °C. The HWLG solution showed superior temperature and salt resistance in comparison with unmodified WLG, due to hydrophobic association-driven network formation. Particularly in formation water, HWLG showed a better long-term thermal stability, retaining 64.5% viscosity after aging 50 d at 70 °C, compared to WLG's 39.6% retention. Core flooding experiments validated HWLG's EOR efficacy, delivering 22.6% incremental oil recovery versus WLG's 13.7%, driven by enhanced mobility control. The integration of hydrophobic functionality endows HWLG with exceptional thermosaline stability, adsorption capacity, and viscoelasticity, positioning it as a robust candidate for high-temperature, high-salinity reservoir flooding applications.

1. Introduction

Petroleum, recognized as the "lifeblood of industrial development", serves as a critical strategic resource that underpins national economic growth and social progress (Sun et al., 2023; Xiang et al., 2025; Ziabakhsh-Ganji et al., 2018). Conventional oil recovery techniques, including primary and secondary extraction methods, typically recover only 30%–40% of original oil in place, leaving approximately 60% of residual oil trapped in complex reservoir formations. To address this challenge and maintain sustainable crude oil production, chemical enhanced oil recovery (EOR) technologies have emerged as a focal point in petroleum engineering research (Afolabi et al., 2022; Liang et al., 2022; Tavakkoli et al., 2022; Wang et al., 2022a). Among various chemical flooding methods, polymer flooding has demonstrated particular technical advantages and operational feasibility (Algharaib et al., 2014; Gbadamosi et al., 2022; Song et al., 2022). This technology has gained global recognition due to its well-defined displacement mechanisms and relatively straightforward implementation processes. Field applications across major oilfields have substantiated that polymer flooding can enhance oil recovery by 8%–15% compared with conventional water flooding. The widespread implementation of this technology has made

* Corresponding author.
** Corresponding author.
E-mail addresses: chenghaoran@qust.edu.cn (H.-R. Cheng), zhaoguang@upc.edu.cn (G. Zhao).
Peer review under the responsibility of China University of Petroleum (Beijing).

https://doi.org/10.1016/j.petsci.2025.12.040

substantial contributions to global energy security, particularly in mature oil fields experiencing production decline, establishing itself as an indispensable component in modern oil recovery technology systems (Guo et al., 2021; Li et al., 2014; Shi et al., 2015).

Polymer flooding enhances oil recovery through two primary mechanisms: (1) mobility control via aqueous phase viscosity modification, which improves the water–oil mobility ratio and increases macroscopic sweep efficiency, and (2) viscoelastic effects that augment microscopic displacement efficiency through polymer chain elongation and subsequent oil droplet mobilization (Chen et al., 2017; Du et al., 2019; Jung et al., 2013). However, the widespread implementation of polymer flooding in conventional reservoirs has substantially depleted the inventory of suitable low-temperature and low-salinity formations. Current industry challenges increasingly focus on high-temperature and high-salinity reservoirs, which now represent over 60% of remaining recoverable resources in mature basins (Hashmet et al., 2017). The technical limitations of conventional EOR polymers become particularly apparent under these harsh reservoir conditions. While partially hydrolyzed polyacrylamide (HPAM) remains the predominant EOR polymer due to its cost-effectiveness and proven performance in mild environments, its practical application faces critical constraints: significant viscosity loss and susceptibility to biological degradation in high-temperature and high-salinity environments (Jin et al., 2020; Kakati et al., 2020; Liu et al., 2021; Panthi and Mohanty, 2024). These constraints necessitate urgent development of novel polymeric systems with enhanced thermal stability and salinity tolerance to satisfy evolving oil production requirements.

Welan gum (WLG), an anionic heteropolysaccharide biosynthesized through microbial fermentation by *Alcaligenes* species, features a triple-helix conformation stabilized by interchain hydrogen bonding. Its repeating unit configuration comprises α-*L*-rhamnopyranosyl termini and α-*L*-mannopyranosyl groups (Liu et al., 2017; Luo et al., 2025; Xu et al., 2013). The unique supramolecular architecture, characterized by intermolecular helical associations, endows WLG solutions with exceptional viscoelastic properties surpassing those of xanthan gum at equivalent concentrations, despite its comparatively lower molecular weight. This biopolymer demonstrates pseudoplastic behavior and superior rheological characteristics, enabling diverse industrial applications spanning food additives, oilfield chemicals, construction materials, and printing formulations (Huang et al., 2022; Massarweh and Abushaikha, 2024). Within petroleum engineering, WLG serves dual functions as a drilling fluid viscosifier and tertiary recovery agent for EOR (Fu et al., 2021; Li et al., 2017; Wang et al., 2023). However, its anionic carboxyl groups render solution properties susceptible to ionic interference. Specifically, Na^+ and Ca^{2+} induce polymer chains shrinkage and coiling through charge screening effects, resulting in the decrease in solution viscosity and viscoelasticity. Elevated temperatures further induce the reduction in WLG solution viscosity through thermal depolymerization of its polysaccharide backbone (Li et al., 2025; Serikov et al., 2025; Xu et al., 2014). This limitation necessitates structural optimization of WLG to enhance its viscoelastic performance under extreme reservoir conditions. As a biodegradable polysaccharide macromolecule, WLG's modification potential originates from its abundant primary hydroxyl groups along the backbone, which enable diverse chemical modifications including oxidation, etherification/esterification, and graft copolymerization (Wang et al., 2020).

Hydrophobically associating polysaccharides/polymers are synthesized through the strategic incorporation of hydrophobic moieties into hydrophilic polymer backbones, predominantly via etherification reactions (Nystrom et al., 2009; Roy et al., 2014; Wang et al., 2022b). These materials develop three-dimensional associative networks through intermolecular hydrophobic interactions, which enhance their resistance to saline environments, elevated temperatures, and shear degradation. Enhanced salt and thermal tolerance has been demonstrated in acrylamide-based copolymers functionalized with 1-bromooctadecane, a long-chain alkyl bromide that facilitates covalent grafting due to its terminal bromine (Wu et al., 2022).

In this study, a hydrophobically modified Welan gum (HWLG) was obtained by grafting 1-bromooctadecane on WLG through an etherification reaction. Comprehensive characterization of the HWLG's chemical structure was performed using Fourier transform infrared spectroscopy (FT-IR), nuclear magnetic resonance spectroscopy (^{1}H-NMR), gel permeation chromatography (GPC), thermogravimetric analysis (TGA), and scanning electron microscopy (SEM). Systematic investigations were conducted to evaluate the solution properties of HWLG, including thickening ability, temperature resistance, salt tolerance, long-term thermal stability, and adsorption capacity. The EOR potential was further assessed through core flooding experiments under simulated reservoir conditions. Analytical results demonstrate that HWLG exhibits promising application prospects as an efficient chemical flooding agent for oil recovery in reservoirs with high temperature and high salinity environments. This study provides fundamental data supporting the development of biopolymer-based EOR agents for challenging reservoir conditions.

2. Experimental section

2.1. Materials

WLG, *N*,*N*-dimethylformamide (DMF), 1-bromooctadecane, KBr, and triethylamine were obtained from Macklin (China). Ethanol, NaCl, $CaCl_2$, and $MgCl_2$ were purchased from Sinopharm Group (China). All chemicals were utilized without further purification. Aqueous solutions were prepared using simulated formation water from the Shengli Oilfield in China, and the ionic composition is presented in Table 1. The crude oil sample was also obtained from the Shengli Oilfield and had a density of 0.84 g·cm^{-3} and a viscosity of 27.85 mPa·s at 25 °C. The artificial core samples were fabricated from compaction-cemented quartz grains within a low-clay-content matrix.

2.2. Synthesis of HWLG

The hydrophobically modified Welan gum (HWLG) was synthesized through an etherification reaction under alkaline conditions. In a typical procedure, a three-necked flask equipped with a mechanical stirrer, a condenser, and a nitrogen inlet/outlet was immersed in a thermostated water bath. Initially, 4.0 g of WLG was uniformly dispersed in 30 mL of anhydrous *N*,*N*-dimethylformamide (DMF) under continuous stirring (500 rpm) at ambient temperature for 12 h to achieve complete polymer swelling and molecular chain disentanglement. The system was subsequently purged with high-purity nitrogen (99.99%) for 15 min to create an inert atmosphere and then heated to 70 °C. Catalytic

Table 1
The formation water composition.

Ion concentration, mg·L^{-1}						Total dissolved solids (TDS), mg·L^{-1}
$Na^+ + K^+$	Ca^{2+}	Mg^{2+}	Cl^-	SO_4^{2-}	HCO_3^-	
3418	409	78	6061	130	105	10,201

deprotonation of the WLG hydroxyl groups was initiated by injecting 1.2 mL of triethylamine into the reaction mixture, which was maintained under these alkaline conditions for 20 min. The alkylation reaction was then performed via the slow, dropwise addition of 2.0 mL of 1-bromooctadecane (dissolved in 5 mL of anhydrous DMF) over a period of 30 min to ensure uniform reaction. After the addition, the system was purged with nitrogen for another 5 min to remove any residual oxygen. The grafting reaction proceeded isothermally at 70 °C for 7 h under a continuous nitrogen blanket. Post-reaction, the crude product was cooled to room temperature, collected by vacuum filtration, and rigorously purified through three successive cycles of washing with anhydrous ethanol and re-precipitation to remove unreacted reagents and byproducts. The final product was dried to a constant weight in a vacuum oven at 80 °C for 24 h. The synthetic route is illustrated in Fig. 1.

2.3. Characterization of the HWLG

The chemical structures and spatial network of HWLG were systematically characterized through FT-IR, ^{1}H NMR, GPC, TGA, and SEM. FT-IR spectra were recorded on an ABB Bomen FTLA2000-104 spectrometer (400–4000 cm^{-1}, 4 cm^{-1} resolution), using KBr pellets prepared by hydraulic compression. The ^{1}H NMR spectrum was recorded on a Bruker Avance300 spectrometer (300 MHz) using deuterium oxide (D_2O) as solvent. Chemical shifts were referenced to residual HOD ($\delta = 4.79$ ppm). The molecular weights and molecular weight distributions of WLG and HWLG were determined by gel permeation chromatography on an Agilent PL-GPC50 system, employing an aqueous mobile phase at a flow rate of 1.0 mL·min^{-1}. The analyses of thermogravimetric behavior of HWLG were executed under nitrogen purge (50 mL·min^{-1}) using a NETZSCH TG 209 F3 instrument, with precisely weighed samples (10.0±0.1 mg) heated from 25 to 800 °C at a heating rate of 10 °C·min^{-1}. Morphological analysis was performed using a JEOL JSM-7500F scanning electron microscope operated at an accelerating voltage of 20 kV. Specimens were prepared by hydrating HWLG in deionized water at concentrations of 2000 and 4000 mg·L^{-1}, followed by lyophilization. The freeze-dried samples were mounted on carbon-coated stubs and sputter-coated with gold to ensure surface conductivity.

2.4. Rheological measurements

Rheological performance serves as a critical evaluation parameter for displacement fluids in chemical EOR operations. Steady-state viscosity measurements were conducted using a Brookfield DV-III viscometer with a constant shear rate of 7.34 s^{-1}. The thickening ability was quantified by comparing the apparent viscosity of WLG and HWLG aqueous solutions at different concentrations at 25 °C. Dynamic rheological characterization was performed using a HAAKE MARS 60 rheometer (20 mm parallel plate geometry, 1 mm gap) under controlled strain conditions. Shear-thinning behavior was evaluated through flow sweeps (0.01–1000 s^{-1}) at 25 °C. Viscoelastic properties were determined via oscillatory frequency sweeps (0.01–10 Hz, 0.1 Pa stress) within the linear viscoelastic regime, recording the storage modulus (G') and the loss modulus (G''). Temperature-dependent viscosity profiles were acquired through temperature ramp tests (25–100 °C, 2 °C·min^{-1}) under constant shear (7.34 s^{-1}). Salt tolerance was assessed by measuring solution viscosity (2000 mg·L^{-1} polymer in NaCl/$CaCl_2$ solutions, 0–100,000 mg·L^{-1}) at 25 and 70 °C. All rheological measurements were performed in triplicate, with a relative standard deviation of <5% between replicates.

2.5. Long-term thermal stability

Long-term thermal stability, a critical determinant of polymer viability in EOR applications, is defined by the ability to sustain viscosity over a minimum 30-d operational lifespan. The temporal viscosity evolution of HWLG and WLG in simulated formation water was systematically monitored under anaerobic conditions at both ambient (25 °C) and elevated (70 °C) temperatures. Triplicate measurements were conducted at each temperature, with reported values representing the statistical mean within a relative error of ±3%, ensuring data reproducibility.

2.6. Adsorption of HWLG

The adsorption capacities of WLG and HWLG on 50-mesh of quartz sand particles were quantified via a Shimadzu UV-1800 ultra violet spectrophotometer using the starch-cadmium iodide colorimetric method (Musa et al., 2023). Polymer concentrations

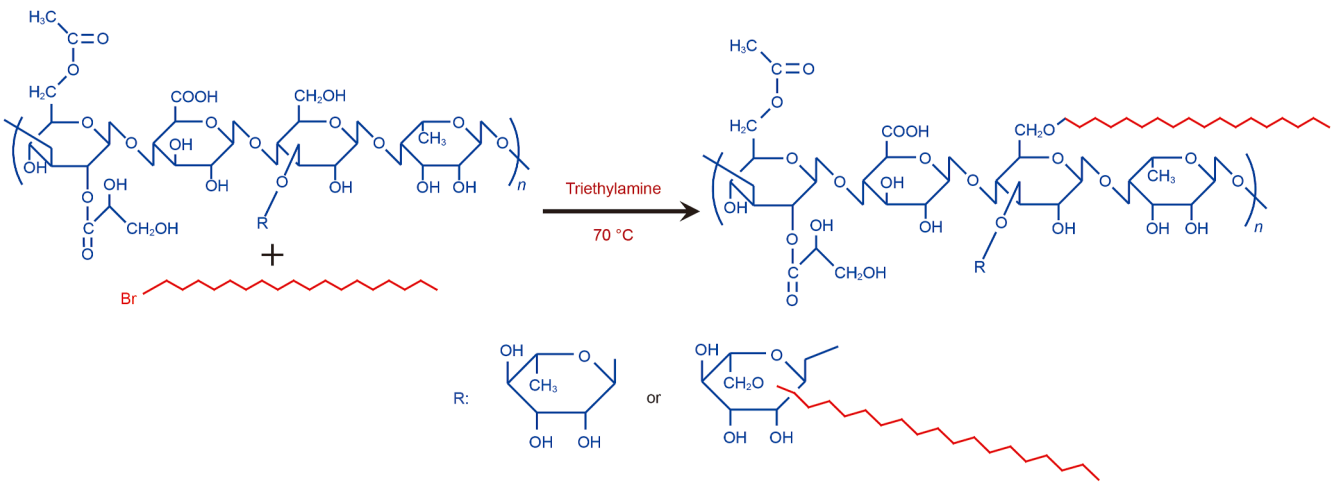

Fig. 1. Synthetic route of HWLG.

were determined by measuring absorbance at roughly 586 nm. Pretreated quartz sand (50-mesh sieve fraction) was rinsed sequentially with deionized water, 0.1 mol·L^{-1} HCl, and ethanol to eliminate surface impurities. Batch adsorption experiments were conducted by mixing 10 g of sand with 50 mL of polymer solutions (gradient concentrations: 250–3500 mg·L^{-1}) in 100 mL conical flasks. The mixtures were subjected to continuous agitation (200 rpm) in a constant temperature oscillator at 70 °C for 24 h to achieve adsorption equilibrium. Post-equilibrium, suspensions were centrifuged (4000 rpm, 15 min), and residual polymer concentrations in supernatants were analyzed. Adsorption capacities of HWLG and WLG were calculated using Eq. (1):

$$\Gamma = \frac{(C_0 - C_e)V}{1000m} \quad (1)$$

where Γ is the adsorption capacity of polymer, mg·g^{-1}; C_0 and C_e denote the initial and equilibrium polymer concentrations, respectively, mg·g^{-1}; V corresponds to the polymer solution volume, L; m represents the mass of quartz sand, g.

2.7. Polymer flooding experiment

Polymer flooding efficacy evaluations were conducted in the artificial sandstone cores to assess the EOR performance of WLG and HWLG solutions under reservoir-simulated conditions (70 °C, 10,201 mg·L^{-1} brine). The schematic diagram of core flooding equipment is detailed in Fig. 2. All cores underwent pretreatment through oven-drying at 90 °C for 24 h prior to polymer flooding experiment. The experimental procedures of polymer flooding include the following steps. (1) The cores were vacuumed for 12 h, saturated with simulated formation water to calculate the water permeability. (2) The crude oil was injected into the cores to establish initial oil saturation. (3) The simulated formation water was injected into the cores with a rate of 0.3 mL·min^{-1} at 70 °C until the water cut surpassed 98%, and the water flooding recovery was calculated. (4) 1.0 PV polymer solution was injected into the cores at equivalent flow rate. (5) Subsequent water flooding was carried out until water cut surpassed 98% again. Solutions of the WLG and HWLG with 2000 mg·L^{-1} were selected to conduct the polymer flooding experiments. Continuous monitoring of injection pressure, produced fluid volume, and the amount of produced crude oil was implemented throughout the displacement procedure to determine the displacement efficiency for each flooding stage.

The water flooding recovery was quantified using Eq. (2), the total oil recovery factor was derived from Eq. (3), and the incremental oil recovery (ΔE) attributable to polymer flooding was calculated through Eq. (4) (Fu et al., 2022).

$$E_1 = \frac{V_1}{V} \times 100\% \quad (2)$$

$$E_2 = \frac{V_2}{V} \times 100\% \quad (3)$$

$$\Delta E = E_2 - E_1 \quad (4)$$

where E_1 is the water flooding recovery; E_2 is the total oil recovery; V_1 is the cumulative oil production during waterflooding, mL; V_2 is the total cumulative oil production, mL; V is the original oil in sand, mL; ΔE is the incremental oil recovery by polymer flooding and subsequent water flooding.

3. Results and discussion

3.1. Characterization

3.1.1. ^{1}H NMR analysis

The ^{1}H NMR (400 MHz, D_2O) spectral characterization of HWLG is presented in Fig. 3. A distinctive triplet observed at $\delta = 0.90$ ppm corresponded to the terminal methyl group (–C**H**$_3$) protons. The aliphatic methylene (–(C**H**$_2$)$_n$–) protons were indicated by the peaks at $\delta = 1.25$–1.61 ppm, with peak multiplicity and integration consistent with extended alkyl chain incorporation. Peaks at $\delta = 2.27$ ppm and $\delta = 3.32$ ppm corresponded to the existence of (–C**H**–) protons and ether methylene (–C**H**$_2$–O–) protons, respectively. The $\delta = 3.51$–3.75 ppm region exhibited overlapping resonances assignable to both the (–C**H**OC–) protons and hydroxyl-bearing carbon (–C**H**(OH)–) protons within the polysaccharide backbone. Notably, the observed signal at $\delta = 4.21$ ppm corresponded to residual hydroxyl (–O**H**) protons. Furthermore, the degree of substitution (DS) was estimated to be 0.105 from the ^{1}H NMR spectrum by comparing the integrated area of the signals from the grafted alkyl chains to those of the polymer backbone. This observed value is in close agreement with the expected degree of substitution of 0.107 calculated from the molar feed ratio of

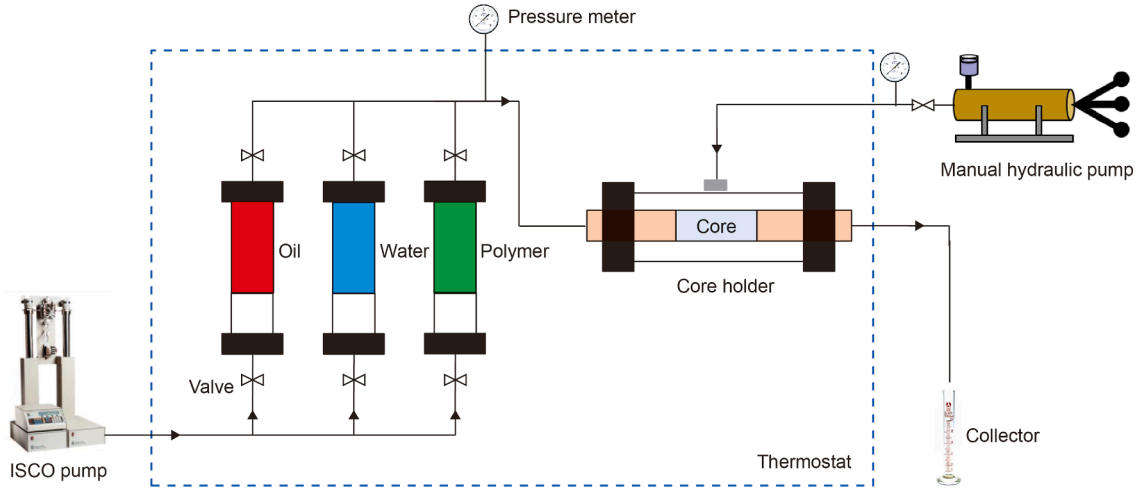

Fig. 2. Schematic diagram of the core-flooding equipment.

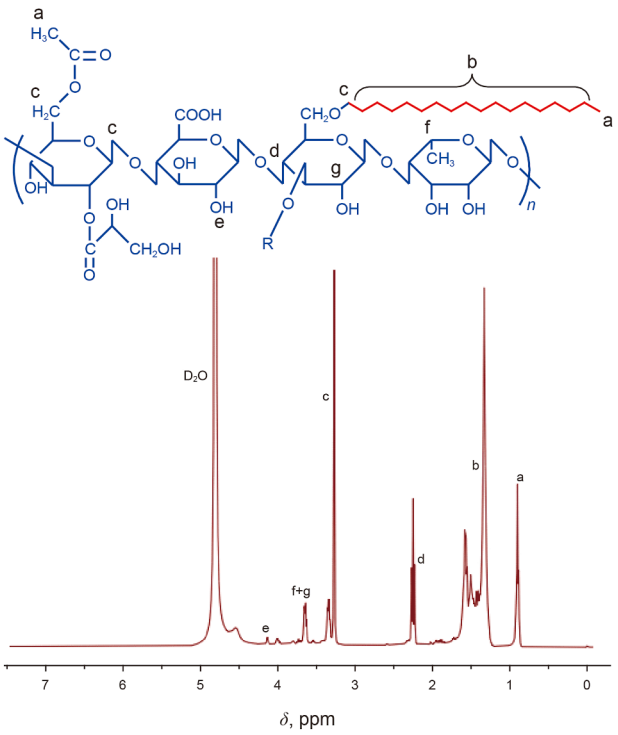

Fig. 3. ^{1}H NMR spectrum of HWLG.

the reactants. This excellent correlation confirms the success of the grafting reaction and highlights its controllable nature (Biswas et al., 2020). These observations, combined with complementary FT-IR data, provide unequivocal confirmation of the target polymer's chemical architecture.

3.1.2. FT-IR spectroscopy analysis

The FT-IR spectra of WLG and its hydrophobically modified derivative HWLG are presented in Fig. 4. In the WLG spectrum, a prominent absorption band at 3439 cm^{-1} was observed, corresponding to the O–H stretching vibration of hydroxyl groups on the polysaccharide ring. Characteristic vibrational absorption bands were identified at 2928 cm^{-1} (C–H stretching vibration in methyl groups), 1628 cm^{-1} (C–O stretching vibration of the alkyl lipid), 1399 cm^{-1} ($-CH_2-$ bending vibration), and 1048 cm^{-1} ($-C-O-C-$ stretching vibration on the glycosidic bond). Notable spectral modifications were observed in the HWLG spectrum. The

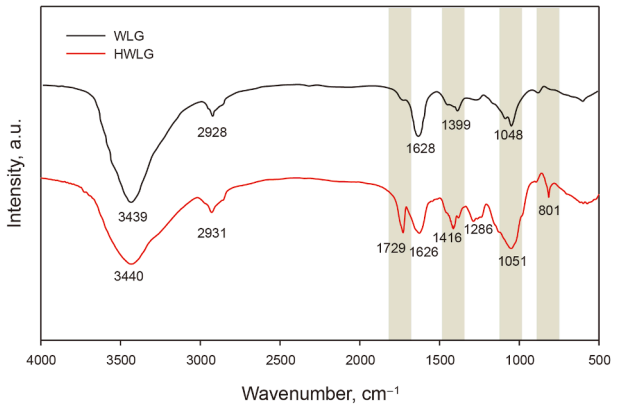

Fig. 4. FT-IR spectra of WLG and HWLG.

absorption band at 1051 cm^{-1} exhibited enhanced intensity, attributed to the combined contributions from glycosidic $-C-O-C-$ stretching and newly formed ether bonds resulting from the chemical modification. A distinct absorption peak emerged at 801 cm^{-1}, corresponding to the rocking vibration of $-(CH_2)_n-$ groups. This vibration mode, typically absent or negligible when the methylene chain contains fewer than three units, became pronounced in HWLG, indicating successful incorporation of extended alkyl chains. Concurrently, the methyl C–H stretching vibration at 1416 cm^{-1} demonstrated significant intensification, likely arising from asymmetric configurations between the original methyl groups and newly introduced long-chain alkyl substituents on the modified polysaccharide backbone. These spectral alterations, particularly the emergence of alkyl chain-associated vibrations and enhanced ether bond signals, provide conclusive evidence for the successful structural modification of WLG through hydrophobic functionalization. The observed peak shifts and intensity changes confirm the establishment of new covalent bonds while maintaining the fundamental polysaccharide architecture.

3.1.3. GPC analysis

Table 2 presents the molecular weights and polydispersity index (PDI) of WLG and HWLG. The modification resulted in a substantial increase in both the number-average molecular weight (M_n), from 795.5 to 1113.4 kDa, and the weight-average molecular weight (M_w), from 1543.1 to 1772.9 kDa. This elevation in molecular weight is a critical factor governing the rheological behavior of polymers. Higher molecular weights promote chain entanglement, shifting the flow unit from the entire chain to shorter segments. The coordinated motion required for these entangled segments to flow results in greater energy dissipation and, consequently, a significant enhancement in viscosity. Furthermore, the PDI of HWLG decreased, indicating a narrower molecular weight distribution. Polymers with a broad molecular weight distribution typically exhibit heightened shear-thinning due to the disproportionate alignment and deformation of the longest chains under shear. In contrast, the more uniform chain length in HWLG contributes to a more stable microstructure under deformation, leading to superior shear resistance.

3.1.4. Thermal stability measurement

The thermal degradation behavior of HWLG was investigated through TGA and derivative thermogravimetry (DTG), as illustrated in Fig. 5. The thermal decomposition profile exhibited two distinct degradation stages. The initial mass loss (10.22%) occurring between 40 and 130 °C corresponds to the volatilization of bound water molecules associated with the disruption of hydrogen-bonding networks within the polysaccharide's hydrophilic domains. The principal degradation event commenced above 246.3 °C, characterized by a maximum mass loss rate of −11.46 %·min^{-1} at 261.9 °C. This secondary stage accounted for 70.21% mass loss, arising from concurrent thermal processes: (1) pyrolytic cleavage of grafted alkyl side chains and (2) depolymerization of the polysaccharide backbone through glycosidic bond scission and functional group decomposition. The residual mass fraction of 19.57% at 800 °C represents thermally stable

Table 2
M_n, M_w, and PDI of WLG and HWLG.

Polymer system	M_n, KDa	M_w, KDa	PDI (M_w/M_n)
WLG	795.5	1543.1	1.94
HWLG	1113.4	1772.9	1.59

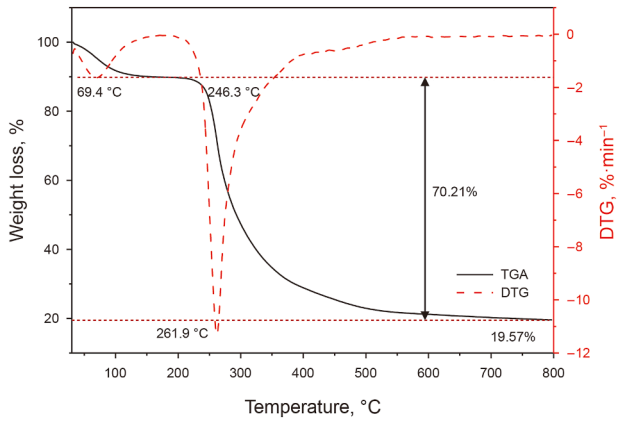

Fig. 5. TGA and DTG curves of HWLG.

carbonaceous products formed during incomplete combustion. The staged decomposition pattern aligns with typical behavior of hydrophobically modified biopolymers, where bound water evaporation precedes structural decomposition of both carbohydrate and alkyl components.

3.1.5. Surface morphology analysis

The aggregation microstructures of WLG and HWLG in aqueous media were systematically investigated through morphological characterization, as depicted in Fig. 6. At a concentration of 2000 mg·L^{-1} in deionized water (Fig. 6(a)), unmodified WLG exhibited extensive lamellar structures with minimal interchain connectivity, demonstrating an absence of three-dimensional network formation between polymer backbones. Hydrophobic modification induced significant morphological reorganization, as evidenced by HWLG (2000 mg·L^{-1}) displaying a well-defined reticulated architecture with ordered spatial arrangement of polymer chains (Fig. 6(b)). As the salinity increased to 10,000 mg·L^{-1} (Fig. 6(c)), the network density increased due to enhanced hydrophobic associations driven by salt-induced polarity elevation, which reinforced the interconnected structure and maintained its integrity (Zhang et al., 2011). Remarkably, even under a high salinity of 60,000 mg·L^{-1} (Fig. 6(d)), although a slight compaction of the network was observed possibly due to enhanced charge screening effect, the three-dimensional network architecture of HWLG remained largely intact, without visible macroscopic precipitation or structural collapse. The morphological transition from lamellar to networked structures, coupled with salinity-enhanced association phenomena, provides direct visual evidence for the successful integration of hydrophobic functionalities and their critical role in governing the supramolecular architecture of modified biopolymers.

3.2. Thickening ability of HWLG

The thickening ability of aqueous solutions, particularly their concentration-dependent rheological behavior, constitute critical performance metrics for polymer flooding applications. Fig. 7 delineates the apparent viscosity profiles of WLG and HWLG solutions at 25 °C as functions of polymer concentration. Both systems showed similar behavior with viscosity escalation upon concentration elevation, though marked divergence emerged beyond critical thresholds. At low concentrations, WLG and HWLG exhibited comparable Newtonian flow characteristics with low viscosity magnitudes, indicative of dominant intrachain interactions over interchain associations in the modified polymer. This regime reflects limited network development due to insufficient chain overlap and hydrophobic group proximity. A rheological transition occurred at the critical association concentration (CAC) of HWLG (2700 mg·L^{-1}), representing a 28.9% reduction

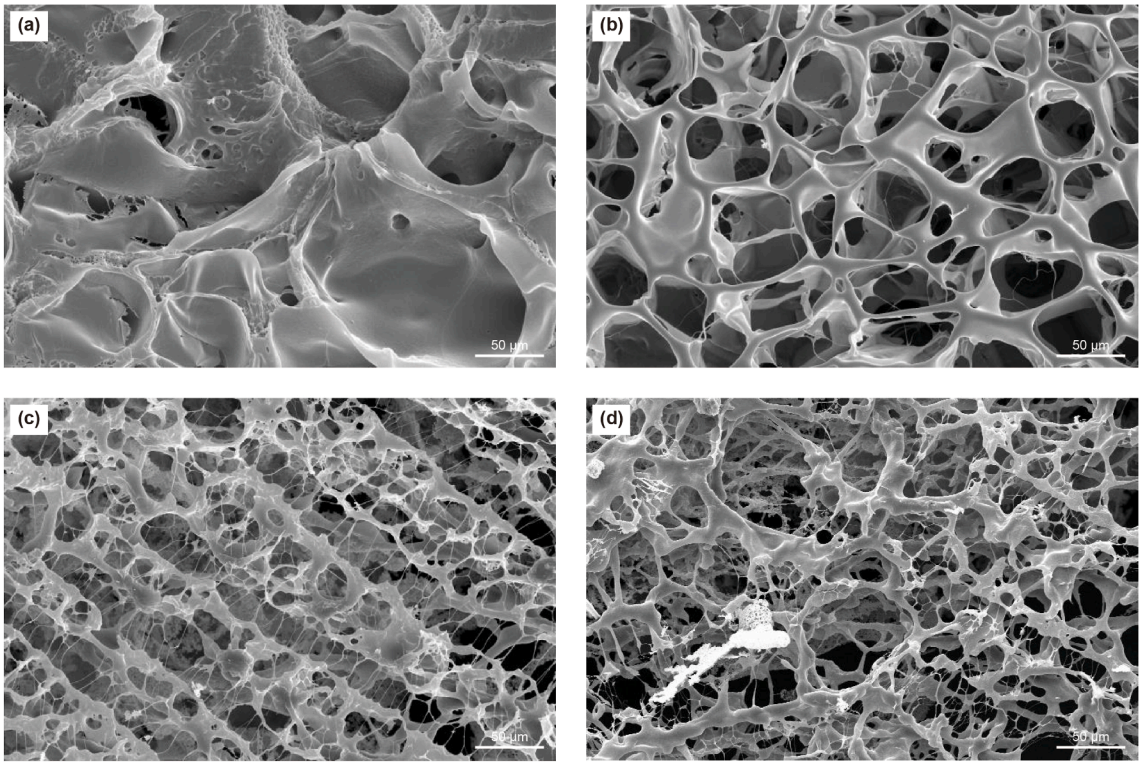

Fig. 6. (**a**) SEM image of WLG (2000 mg·L^{-1}) in deionized water. SEM images of HWLG (2000 mg·L^{-1}) in deionized water (**b**), 10,000 (**c**) and 60,000 (**d**) mg·L^{-1} saline water.

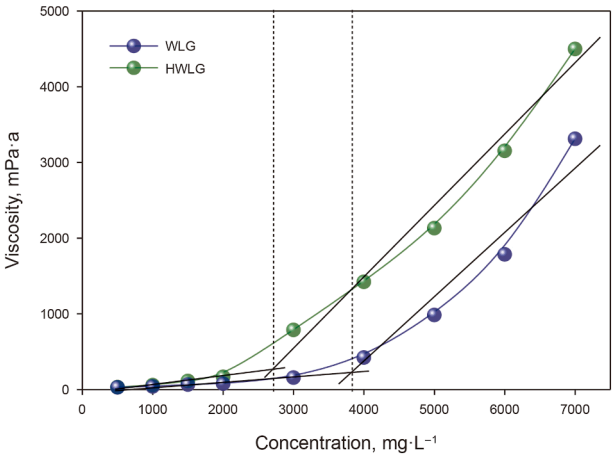

Fig. 7. Effect of polymer concentration on the apparent viscosity of WLG and HWLG.

from WLG's CAC (3800 mg·L^{-1}). Beyond this threshold, HWLG displayed exponential viscosity enhancement, achieving 1423.2 mPa·s at 4000 mg·L^{-1}, a 3.4-fold increase over unmodified WLG at equivalent concentration. This phenomenon arises from hydrophobic association mediated by alkyl chains, wherein strengthened intermolecular interactions promote the expansion of the association network volume and the increase in the association network numbers (Wever et al., 2011). The concurrent increase in both spatial dimensions and density of association network synergistically amplified the macroscopic viscosity response.

3.3. Temperature resistance of HWLG

The temperature-dependent viscoelastic behavior of WLG and HWLG (2000 mg·L^{-1}) in deionized water and simulated formation water is illustrated in Fig. 8. Both systems exhibited progressive viscosity reduction with increasing temperature, a phenomenon governed by thermally activated molecular dynamics. This inverse temperature–viscosity correlation stems from the following synergistic mechanisms. First, the intensified Brownian motion of the hydrophobic group disrupted the hydrophobic association. Second, the reduced hydration of hydrophilic groups promoted chain shrinkage. Besides, thermal scission of labile bonds within the polymer backbone compromised network integrity. Notably, HWLG demonstrated superior temperature resistance performance, maintaining significantly higher viscosity retention across the tested temperature range (25–110 °C) compared to WLG. The incorporated hydrophobic moieties of HWLG introduce an additional, robust associative mechanism. The hydrophobic associations, being entropically driven (hydrophobic effect), exhibit a non-covalent character that is inherently less susceptible to thermal degradation compared to covalent bonds. Although elevated temperature increases the kinetic energy of polymer chains, which can temporarily disrupt individual hydrophobic junctions, the dynamic and reversible nature of these associations allows for rapid re-formation upon cooling or even at elevated temperatures, thereby maintaining the overall network integrity. In contrast, the degradation of WLG upon heating is more irreversible, primarily involving the permanent scission of glycosidic bonds in the polysaccharide backbone and the collapse of its hydrogen-bond-stabilized helical structure. Furthermore, HWLG in simulated formation water exhibited enhanced viscosity relative to deionized water counterparts, attributable to salinity-induced polarity elevation strengthening hydrophobic interactions. The amplified associative forces between alkyl grafts in saline environments partially counteracted thermal degradation effects, highlighting the material's dual resistance to thermal and saline challenges (Viken et al., 2018). These findings collectively confirm that hydrophobic modification confers enhanced structural stability, positioning HWLG as a promising candidate material for high-temperature reservoir applications.

3.4. Salt tolerance of HWLG

The salinity-dependent viscoelastic properties of WLG and HWLG solutions (2000 mg·L^{-1}) were systematically investigated under isothermal conditions (25 and 70 °C) across varying ionic types of NaCl and $CaCl_2$, as presented in Fig. 9. Distinct cation valence effects were observed, with divalent ions (Ca^{2+}) exerting more pronounced impacts on the viscosity of polymer solution than monovalent counterparts (Na^+). Unmodified WLG exhibited contrasting salinity responses: progressive viscosity reduction in NaCl solutions versus a nonmonotonic profile in $CaCl_2$ characterized by initial viscosity enhancement followed by sharp decline. This phenomenon likely originates from competitive interactions between Ca^{2+} and carboxyl groups in WLG's backbone, where low concentrations induce transient crosslinking through cation bridging, while excessive divalent ions promote charge screening and chain collapse (Zhang et al., 2019). In contrast, HWLG

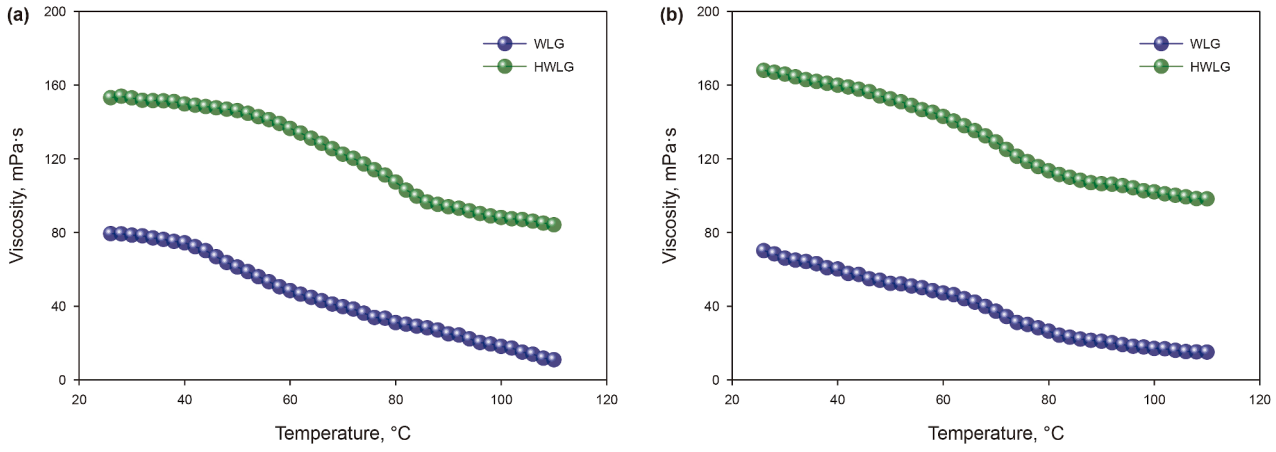

Fig. 8. Effect of temperature on the apparent viscosity of WLG and HWLG in deionized water (**a**) and simulated formation water (**b**).

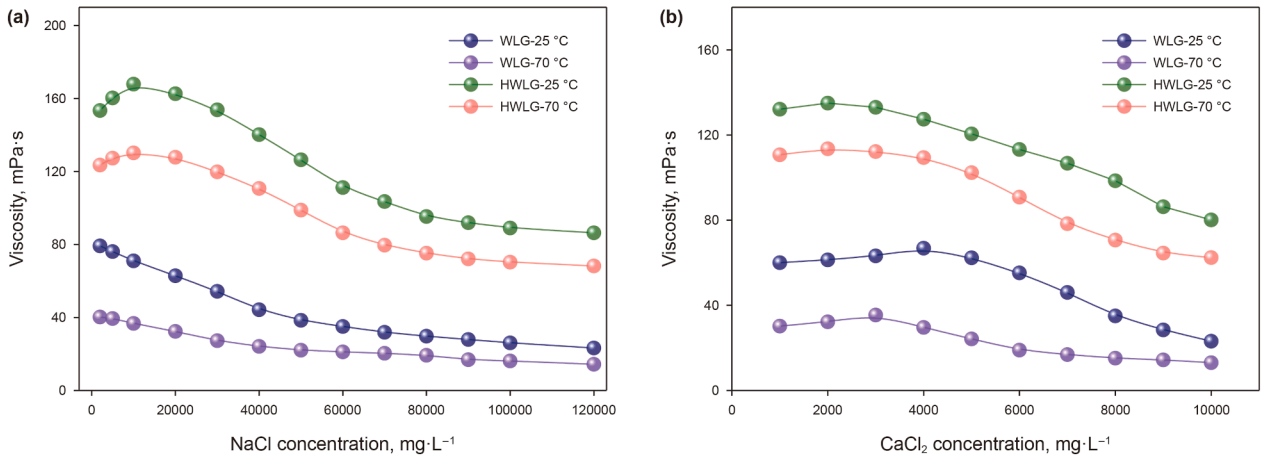

Fig. 9. Effect of salinity on the apparent viscosity of WLG and HWLG in NaCl solution (**a**) and $CaCl_2$ solution (**b**) measured at 25 and 70 °C.

demonstrated superior ionic stability, maintaining elevated viscosity magnitudes in both saline systems. At extreme salinities (120,000 mg·L^{-1} NaCl and 10,000 mg·L^{-1} $CaCl_2$), HWLG retained over 55% of its initial viscosity, whereas WLG viscosity dropped below 30%. This confirms HWLG's robustness in hypersaline environments. The exceptional salt tolerance of HWLG stems from a fundamental shift in the dominant stabilization mechanism from electrostatic repulsion to hydrophobic association. Unmodified WLG, as a polyelectrolyte, relies on charge repulsion along its backbone to maintain an extended chain conformation. The addition of salts screens these charges, leading to chain coiling and catastrophic viscosity loss. For HWLG, the introduction of hydrophobic groups provides an alternative, salt-insensitive crosslinking mechanism. Notably, HWLG solutions exhibited salt-thickening behavior at low salinity, with viscosity enhancement driven by salt-induced polarity elevation amplifying hydrophobic associations between alkyl grafts. This associative networking effect predominated until critical salinity thresholds (10,000 mg·L^{-1} for NaCl, 2000 mg·L^{-1} for $CaCl_2$), beyond which excessive cations disrupted network integrity through electrostatic screening effect and chain compaction. Furthermore, the attenuated salt-thickening efficacy in $CaCl_2$ versus NaCl systems stems from amplified charge screening by divalent cations, which effectively neutralize anionic backbone charges at lower ionic concentrations (Lu et al., 2018). The remarkable salt tolerance of HWLG underscores the effectiveness of the hydrophobic association in creating a robust, physically crosslinked network that is less dependent on electrostatic repulsion for its stability. HWLG's preserved rheological performance under combined ionic and thermal condition confirms the structural stability imparted by dynamic hydrophobic crosslinks, highlighting its potential for high-salinity reservoir applications.

3.5. Rheological property of HWLG

The shear-dependent rheological properties of 2000 mg·L^{-1} WLG and HWLG in deionized water and simulated formation water were characterized across a shear rate range of 0.01–1000 s^{-1}, as shown in Fig. 10(a). Both systems exhibited characteristic shear-thinning behavior of pseudoplastic fluids, with viscosity inversely correlated to shear rate. Notably, HWLG in simulated formation water demonstrated enhanced low-shear viscosity (<10 s^{-1}) relative to deionized water counterparts. This salinity-induced viscosity amplification diminished at elevated shear rates, where the addition of salt amplified shear-thinning effect through disruption of hydrophobic association under high shear stress. Fig. 10(b) shows the storage modulus (G') and the loss modulus (G'') of the WLG and HWLG with 2000 mg·L^{-1} concentration in deionized water and simulated formation water. The viscoelastic modulus analysis revealed distinct mechanical responses between polymer systems. For unmodified WLG in simulated formation water, G'' was higher than G' at low frequencies, revealing liquid-dominated behavior dominated by viscous dissipation. With increasing shear frequency, both modulii exhibited progressive increase until intersecting at a critical frequency, beyond which elastic behavior dominated ($G' > G''$) in the high-frequency regime. In marked contrast, HWLG in deionized water and simulated formation water persistently exhibited $G' > G''$ from 0.1 to 10 Hz, demonstrating elastic dominance throughout the entire tested frequency range. Notably, both modulus (G' and G'') of HWLG in simulated formation water were higher than those in deionized water, attributable to salinity-enhanced hydrophobic association. This frequency-dependent rheological behavior, characteristic of entangled polymer networks with energy-dissipative features, originates from physical crosslinking via hydrophobic association complexes. The marked enhancement of both modulus in HWLG relative to WLG confirms the establishment of interconnected associative networks, endowing the modified polymer with pronounced viscoelastic gel characteristics.

3.6. Long-term thermal stability

The long-term aging stability of polymeric agents under simultaneous thermal and saline stress is a critical determinant of their viability and practical efficacy in EOR applications, particularly given the inevitable degradation and chain scission occurring during extended reservoir exposure (Gou et al., 2017). To assess this property, WLG and HWLG (2000 mg·L^{-1}) in simulated formation water were subjected to isothermal aging at 25 and 70 °C under sealed conditions for 50 d. Fig. 11 illustrated the temporal evolution of solution viscosity under these conditions. It was observed that after 50 d of aging at 70 °C, the viscosity of HWLG solution decreased from 132.1 to 85.2 mPa·s with a viscosity retention rate of 64.5%, whereas the viscosity of WLG solution decreased from 39.6 to 15.7 mPa·s, and the viscosity retention rate was only 39.6%. The remarkable long-term stability of HWLG under such harsh conditions (70 °C, 10,201 mg·L^{-1} TDS) is directly attributable to its associative network structure. The hydrophobic junctions, while dynamic, create a physical barrier that slows

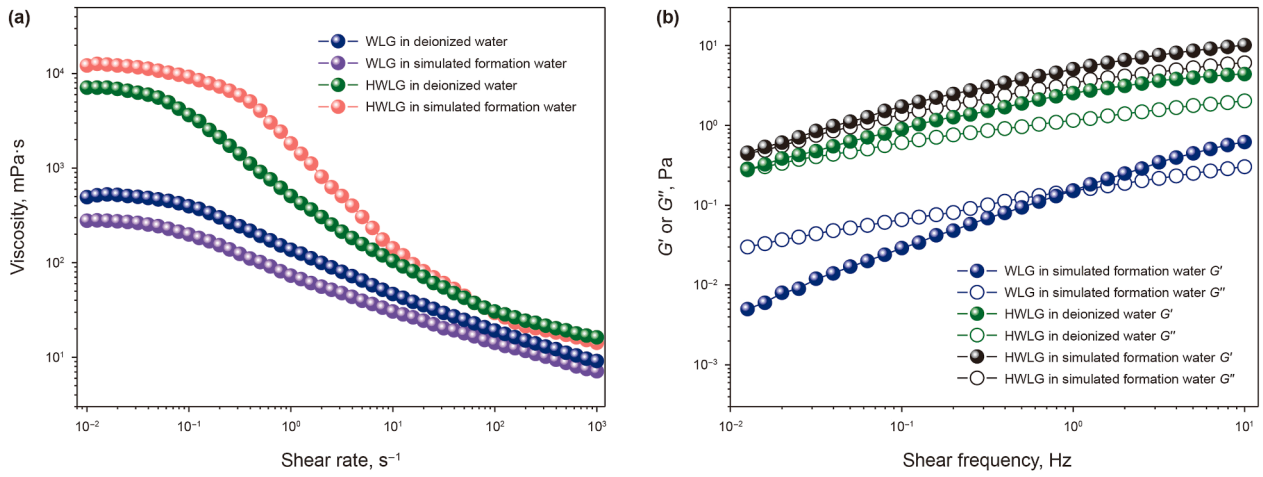

Fig. 10. The rheological properties of WLG and HWLG in deionized water and simulated formation water. (**a**) Effect of shear rate on apparent viscosities of polymer solutions. (**b**) Modulus curves as a function of frequencies for polymer solutions.

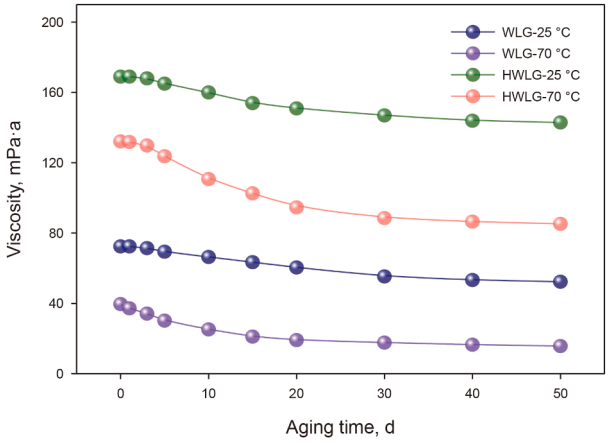

Fig. 11. The long-term thermal stability of WLG and HWLG in simulated formation water at different temperatures (25 and 70 °C).

down the hydrolytic degradation of the polysaccharide backbone. Furthermore, the network's ability to dissipate energy through the reversible breakage and re-formation of associations helps to maintain macroscopic viscosity over time. The comparative data conclusively establish HWLG's superior long-term thermal stability relative to unmodified WLG, underscoring its potential viability for extended-duration polymer flooding operations in high-temperature and high-salinity reservoirs.

3.7. Adsorption of HWLG

The adsorption characteristics of WLG and HWLG were quantitatively analyzed through spectrophotometric calibration and adsorption isotherm studies, as illustrated in Fig. 12. A linear correlation ($R^2 > 0.99$) between polymer concentration and absorbance was established for both systems (Fig. 12(a)), validating the precision of the analytical methodology. Adsorption equilibrium studies (Fig. 12(b)) revealed concentration-dependent adsorption curves, where adsorption capacity increased asymptotically with rising polymer concentration. When the concentration increased to 2500 mg·L^{-1}, the adsorption capacity tended to be stable. Comparative analysis demonstrated that the adsorption capacity of HWLG was higher than WLG during the entire range of tested concentrations of polymer. It can be calculated that the equilibrium adsorption amount of WLG and HWLG were 4.28 and 5.41 mg·g^{-1}, respectively. This elevation arises from the hydrophobic interactions between HWLG's grafted alkyl chains and oil-wet reservoir rock surfaces, promoting interfacial adhesion of HWLG. Besides, reduced electrostatic repulsion due to charge screening by hydrophobic domains facilitates polymer-surface contact. The reinforced adsorption of HWLG correlates directly with enhanced residual resistance in porous media. Increased polymer retention at fluid–rock interfaces establishes higher flow resistance coefficients, effectively modulating mobility ratios and improving macroscopic sweep efficiency during water flooding.

3.8. Polymer flooding for EOR

Dynamic core flooding experiments were carried out to evaluate the EOR ability of WLG and HWLG (2000 mg·L^{-1}) at 70 °C, with basic parameters of the core used and experimental outcomes detailed in Table 3 and Fig. 13. Initial water flooding achieved 52.7%–53.2% recovery efficiency, establishing a consistent baseline for comparative polymer flooding analysis. Post-polymer injection induced rapid water cut reduction and substantial injection pressure elevation, indicative of effective high-permeability channel blockage and improved mobility control, particularly pronounced in HWLG systems. Final oil recovery factors demonstrated significant divergence. WLG yielded 66.4% total oil recovery, representing a 13.7% increase over water flooding. In contrast, HWLG achieved 75.8% ultimate oil recovery (22.6% incremental), demonstrating its excellent EOR ability. The greater incremental recovery from HWLG versus WLG directly correlates with its robust hydrophobic associative networks, as evidenced by rheological and adsorption analyses. These networks maintain pseudoplastic behavior under reservoir conditions, facilitating deep permeability modification while resisting mechanical degradation. The combined mobility control and residual resistance effects confirm HWLG's potential for recovering oil in mature reservoirs, particularly in high-temperature, high-salinity formations where conventional biopolymers exhibit limited stability.

To further decouple the effect of solution viscosity from the intrinsic viscoelastic and adsorption properties of the polymer, an additional core flooding experiment was conducted. In this experiment, the concentration of WLG was increased to

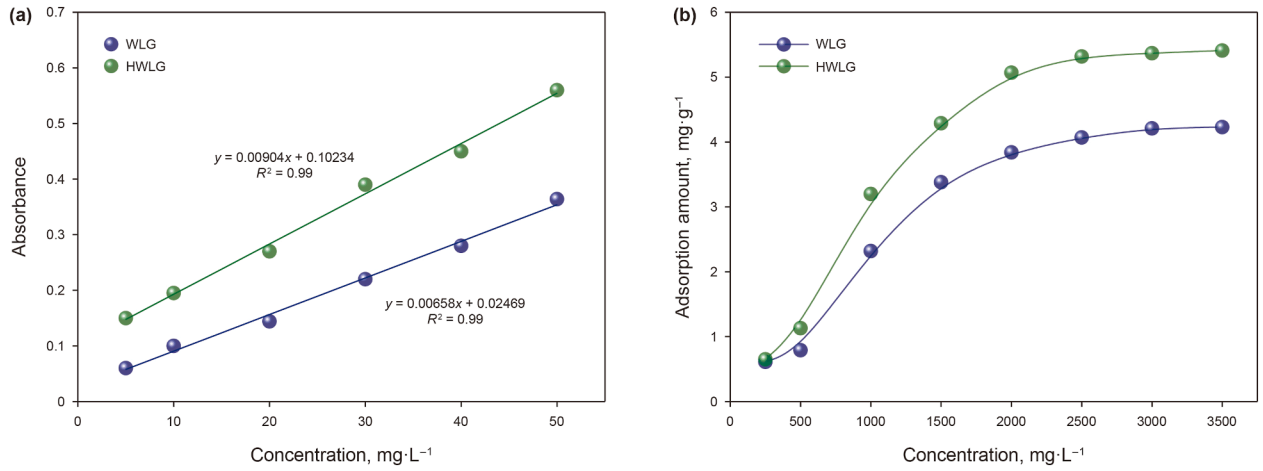

Fig. 12. (**a**) The standard lines of WLG and HWLG. (**b**) The concentration-dependent adsorption curves of WLG and HWLG.

Table 3
Basic parameters of artificial sandstone cores.

Polymer system	Length, cm	Diameter, cm	Permeability, 10^{-3} μm^2	Pore volume, mL	Oil saturation, %	E_1, %	E_2, %	ΔE, %
HWLG	7.55	2.525	140.6	7.82	78.9	53.2	75.8	22.6

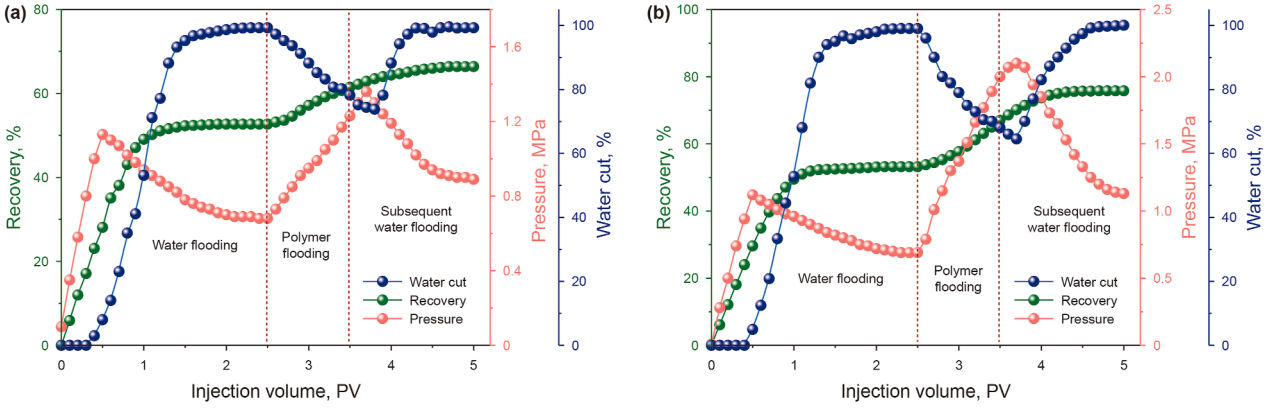

Fig. 13. Polymer flooding results of WLG (**a**) and HWLG (**b**).

Table 4
Core flooding results at equivalent viscosity.

Polymer system	Polymer concentration, mg·L^{-1}	Viscosity, mPa·s	ΔE, %
WLG	3200	170.5	16.1
HWLG	2000	168.2	22.6

3200 mg·L^{-1} to achieve an apparent viscosity (approximately 170 mPa·s) comparable to that of a 2000 mg·L^{-1} HWLG solution. Despite the matched initial viscosity, the oil displacement efficiencies differed significantly. As shown in Table 4 and Fig. 14, the incremental oil recovery achieved by the high-concentration WLG solution was 16.1%, which was still lower than the incremental oil recovery (22.6%) obtained using the HWLG solution at equivalent viscosity. This result clearly demonstrates that the superior EOR performance of HWLG is not solely attributable to its thickening ability. The enhanced recovery is primarily driven by its unique hydrophobic association mechanism, which confers stronger

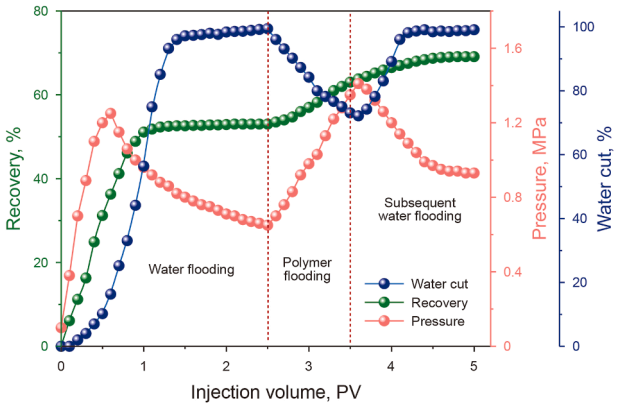

Fig. 14. Polymer flooding results of WLG with concentration of 3200 mg·L^{-1}.

viscoelasticity and higher adsorption capacity on rock surfaces. The associative network endows the polymer solution with significant elastic modulus (G'), which improves the microscopic

displacement efficiency by exerting stronger pulling and deformation forces on disconnected oil ganglia. Simultaneously, the increased viscosity of the displacing fluid and adsorption of HWLG on the rock surface establishes a more substantial residual resistance factor, effectively plugging swept high-permeability channels and diverting the displacing fluid into unswept oil-bearing zones, thereby significantly improving the macroscopic sweep efficiency.

4. Conclusions

In this work, a hydrophobically modified biopolymer HWLG was synthesized through etherification of WLG with 1-bromooctadecane. Structural characterization via FT-IR, ^{1}H NMR, GPC, TGA, and SEM confirmed successful alkyl chain incorporation. The modified biopolymer exhibited superior aqueous solution properties, demonstrating a significant viscosity enhancement through hydrophobic association-driven network formation. Rheological evaluations confirmed exceptional temperature resistance, salt tolerance and long-term thermal stability. Dynamic adsorption studies revealed higher saturated adsorption capacity for HWLG relative to unmodified WLG, primarily ascribed to enhanced alkyl-substrate interfacial interactions. Increased polymer retention at fluid–rock interfaces establishes a greater residual resistance, thereby effectively regulating mobility ratios and enhancing macroscopic sweep efficiency during water flooding. Core flooding experiments demonstrated EOR potential of HWLG through effective mobility control, achieving a 22.6% incremental oil recovery factor. These findings position HWLG as a promising candidate for chemical EOR applications in challenging high-temperature and high-salinity reservoirs, addressing critical limitations of conventional biopolymer thickeners through rational molecular design.

CRediT authorship contribution statement

Jia Chen: Writing – review & editing, Writing – original draft, Investigation, Formal analysis, Data curation, Conceptualization. **Zhao-Kai Wang:** Validation, Investigation. **Wan-Lei Geng:** Formal analysis, Data curation. **Hao-Ran Cheng:** Methodology, Investigation. **Guang Zhao:** Writing – review & editing, Writing – original draft, Formal analysis.

Conflict of interest

The article is original. The article has been written by the stated authors who are all aware of its content and approve its submission. The article has not been published previously. The article is not under consideration for publication elsewhere. No conflict of interest exists. If accepted, the article will not be published elsewhere in the same form, in any language, without the written consent of the publisher.

Acknowledgements

This study is financially supported by the Joint Funds of the National Natural Science Foundation of China (U23B2087), the Fundamental Research Funds for the Central Universities (23CX07003A), and the National Natural Science Foundation of China (52104028).

References

Afolabi, F., Mahmood, S.M., Yekeen, N., Akbari, S., Sharifigaliuk, H., 2022. Polymeric surfactants for enhanced oil recovery: A review of recent progress. J. Pet. Sci. Eng. 208. https://doi.org/10.1016/j.petrol.2021.109358.

Algharaib, M., Alajmi, A., Gharbi, R., 2014. Improving polymer flood performance in high salinity reservoirs. J. Pet. Sci. Eng. 115, 17–23. https://doi.org/10.1016/j.petrol.2014.02.003.

Biswas, A., Cheng, H., Kim, S., Alves, C.R., Furtado, R.F., 2020. Hydrophobic modification of cashew gum with alkenyl succinic anhydride. Polymers 12 (3), 514. https://doi.org/10.3390/polym12030514.

Chen, X., Feng, Q., Liu, W., Sepehrnoori, K., 2017. Modeling preformed particle gel surfactant combined flooding for enhanced oil recovery after polymer flooding. Fuel 194, 42–49. https://doi.org/10.1016/j.fuel.2016.12.075.

Du, Q.J., Pan, G.M., Hou, J., Guo, L.L., Wang, R.R., Xia, Z.Z., Zhou, K., 2019. Study of the mechanisms of streamline-adjustment-assisted heterogeneous combination flooding for enhanced oil recovery for post-polymer-flooded reservoirs. Pet. Sci. 16 (3), 606–618. https://doi.org/10.1007/s12182-019-0311-0.

Fu, L., Jiang, L., Liao, K., An, J., Huang, W., Sun, X., Li, T., He, Y., 2021. Adsorption behavior of welan gum on quartz sand in reservoir. J. Pet. Sci. Eng. 205. https://doi.org/10.1016/j.petrol.2021.108850.

Fu, X., Qin, F., Liu, T., Zhang, X., 2022. Enhanced oil recovery performance and solution properties of hydrophobic associative xanthan gum. Energy Fuels. 36 (1), 181–194. https://doi.org/10.1021/acs.energyfuels.1c02941.

Gbadamosi, A., Patil, S., Kamal, M.S., Adewunmi, A.A., Yusuff, A.S., Agi, A., Oseh, J., 2022. Application of polymers for chemical enhanced oil recovery: A review. Polymers 14 (7). https://doi.org/10.3390/polym14071433.

Gou, S., Li, S., Feng, M., Zhang, Q., Pan, Q., Wen, J., Wu, Y., Guo, Q., 2017. Novel biodegradable graft-modified water-soluble copolymer using acrylamide and konjac glucomannan for enhanced oil recovery. Ind. Eng. Chem. Res. 56 (4), 942–951. https://doi.org/10.1021/acs.iecr.6b04649.

Guo, H., Song, K., Liu, S., Zhao, F., Wang, Z., Xu, Y., Liu, J., Tang, E., Yang, Z., 2021. Recent advances in polymer flooding in China: Lessons learned and continuing development. SPE J. 26 (4), 2038–2052. https://doi.org/10.2118/204455-pa.

Hashmet, M.R., AlSumaiti, A.M., Qaiser, Y., AlAmeri, W.S., 2017. Laboratory investigation and simulation modeling of polymer flooding in high-temperature, high-salinity carbonate reservoirs. Energy Fuels. 31 (12), 13454–13465. https://doi.org/10.1021/acs.energyfuels.7b02704.

Huang, H., Lin, J., Wang, W., Li, S., 2022. Biopolymers produced by *sphingomonas* strains and their potential applications in petroleum production. Polymers 14 (9). https://doi.org/10.3390/polym14091920.

Jin, F.Y., Li, Q.H., He, Y., Luo, Q., Pu, W.F., 2020. Experimental study on enhanced oil recovery method in tahe high-temperature and high-salinity channel sand reservoir: Combination of profile control and chemical flooding. ACS Omega 5 (11), 5657–5665. https://doi.org/10.1021/acsomega.9b03306.

Jung, J.C., Zhang, K., Chon, B.H., Choi, H.J., 2013. Rheology and polymer flooding characteristics of partially hydrolyzed polyacrylamide for enhanced heavy oil recovery. J. Appl. Polym. Sci. 127 (6), 4833–4839. https://doi.org/10.1002/app.38070.

Kakati, A., Kumar, G., Sangwai, J.S., 2020. Low salinity polymer flooding: Effect on polymer rheology, injectivity, retention, and oil recovery efficiency. Energy Fuels. 34 (5), 5715–5732. https://doi.org/10.1021/acs.energyfuels.0c00393.

Li, H., Liu, H., Jia, Y., Li, B., Zhang, Z., Qin, L., Jiang, Y., Wang, D., Sun, Y., Zhu, H., Wang, J., 2025. Preparation and characterization of the octenyl succinic anhydride (OSA) modified sphingan WL gum as novel biopolymeric surfactants. Int. J. Biol. Macromol. 296. https://doi.org/10.1016/j.ijbiomac.2025.139608.

Li, K., Sun, W., Li, F., Qu, Y., Yang, Y., 2014. Novel method for characterizing single-phase polymer flooding. SPE J. 19 (4), 695–702. https://doi.org/10.2118/152988-pa.

Li, Y., Xu, L., Gong, H., Ding, B., Dong, M., Li, Y., 2017. A microbial exopolysaccharide produced by *sphingomonas* species for enhanced heavy oil recovery at high temperature and high salinity. Energy Fuels. 31 (4), 3960–3969. https://doi.org/10.1021/acs.energyfuels.6b02923.

Liang, T., Hou, J.R., Qu, M., Xi, J.X., Raj, I., 2022. Application of nanomaterial for enhanced oil recovery. Pet. Sci. 19 (2), 882–899. https://doi.org/10.1016/j.petsci.2021.11.011.

Liu, X., Zhu, P., Jiang, R., Wu, L., Feng, X., Li, S., Xu, H., 2017. Enhancement of welan gum production in *Sphingomonas* sp HT-1 via heterologous expression of *Vitreoscilla* hemoglobin gene. Carbohydr. Polym. 156, 135–142. https://doi.org/10.1016/j.carbpol.2016.08.081.

Liu, Y., Zhang, J., Wu, X., Kang, X., Guan, B., Li, X., Ye, Y., Xiao, P., Wang, X., Li, S., 2021. Experimental investigation on a novel particle polymer for enhanced oil recovery in high temperature and high salinity reservoirs. J. Chem. 2021. https://doi.org/10.1155/2021/5593038.

Lu, Y., Wu, H., Meng, Z., Jiang, J., Jin, Y., Deng, Z., Su, W., Li, Z., Kang, W., 2018. Salt effect on hydrophobically modified polyacrylamide-containing crude oil emulsions: Stability and rheology study. Colloid Polym. Sci. 296 (3), 515–527. https://doi.org/10.1007/s00396-018-4267-1.

Luo, H., Wang, F., Wang, L., Li, Y., Yang, M., Zhang, H., 2025. Microbial welan gum production, chemistry and applications: A review. Int. J. Biol. Macromol. 306. https://doi.org/10.1016/j.ijbiomac.2025.141640.

Massarweh, O., Abushaikha, A.S., 2024. Towards environmentally sustainable oil recovery: The role of sustainable materials. Energy Rep. 12, 95–119. https://doi.org/10.1016/j.egyr.2024.06.013.
Musa, M.S.M., Agi, A., Nwaichi, P.I., Ridzuan, N., Mahat, S.Q.A.B., 2023. Simulation study of polymer flooding performance: Effect of salinity, polymer concentration in the Malay Basin. Geoenergy Sci. Eng. 228. https://doi.org/10.1016/j.geoen.2023.211986.
Nystrom, B., Kjoniksen, A.L., Beheshti, N., Zhu, K., Knudsen, K.D., 2009. Rheological and structural aspects on association of hydrophobically modified polysaccharides. Soft Matter 5 (7), 1328–1339. https://doi.org/10.1039/b817349d.
Panthi, K., Mohanty, K.K., 2024. Surfactant-polymer flood with seawater for a high temperature carbonate reservoir. Colloid Surf. A-Physicochem. Eng. Asp. 688. https://doi.org/10.1016/j.colsurfa.2024.133615.
Roy, A., Comesse, S., Grisel, M., Hucher, N., Souguir, Z., Renou, F., 2014. Hydrophobically modified xanthan: An amphiphilic but not associative polymer. Biomacromolecules 15 (4), 1160–1170. https://doi.org/10.1021/bm4017034.
Serikov, G., Zhuniskenov, Y., Abbas, A.H., Pourafshary, P., 2025. Synergistic application of Welan gum and polysaccharides for enhanced oil recovery. J. Pet. Explor. Prod. Technol. 15 (3). https://doi.org/10.1007/s13202-025-01955-3.
Shi, L.T., Zhu, S.J., Zhang, J., Wang, S.X., Xue, X.S., Zhou, W., Ye, Z.B., 2015. Research into polymer injection timing for Bohai heavy oil reservoirs. Pet. Sci. 12 (1), 129–134. https://doi.org/10.1007/s12182-014-0012-7.
Song, K., Tao, J., Lyu, X., Xu, Y., Liu, S., Wang, Z., Liu, H., Zhang, Y., Fu, H., Meng, E., Liu, M., Guo, H., 2022. Recent advances in polymer flooding in China. Molecules 27 (20). https://doi.org/10.3390/molecules27206978.
Sun, N., Yao, X., Liu, J., Li, J., Yang, N., Zhao, G., Dai, C., 2023. Breakup and coalescence mechanism of high-stability bubbles reinforced by dispersed particle gel particles in the pore-throat micromodel. Geoenergy Sci. Eng. 223. https://doi.org/10.1016/j.geoen.2023.211513.
Tavakkoli, O., Kamyab, H., Shariati, M., Mohamed, A.M., Junin, R., 2022. Effect of nanoparticles on the performance of polymer/surfactant flooding for enhanced oil recovery: A review. Fuel 312. https://doi.org/10.1016/j.fuel.2021.122867.
Viken, A.L., Skauge, T., Svendsen, P.E., Time, P.A., Spildo, K., 2018. Thermothickening and salinity tolerant hydrophobically modified polyacrylamides for polymer flooding. Energy Fuels. 32 (10), 10421–10427. https://doi.org/10.1021/acs.energyfuels.8b02026.
Wang, H., Chen, F., Li, D., Zhang, L., Luo, M., He, J., Zhong, C., 2022. Viscosity and structure characterization of the 1-bromohexadecane-modified welan gum in the saline solution. Energy Fuels. 36 (12), 6597–6605. https://doi.org/10.1021/acs.energyfuels.2c00580.
Wang, H., Chen, F., Zhan, S., Zhang, L., He, J., Luo, M., Wen, R., Zhong, C., 2023. Synergistic effect of hydrophobic modified Welan gum and sodium alcohol ether sulphate in saline solution. Colloid Surf. A-Physicochem. Eng. Asp. 677. https://doi.org/10.1016/j.colsurfa.2023.132379.
Wang, R., Pu, W., Dang, S., Jiang, F., Zhao, S., 2020. Synthesis and characterization of a graft-modified copolymer for enhanced oil recovery. J. Pet. Sci. Eng. 184. https://doi.org/10.1016/j.petrol.2019.106473.
Wang, Y., Yu, W., Liu, S., 2022b. Physically cross-linked gellan gum/hydrophobically associated polyacrylamide double network hydrogel for cartilage repair. Eur. Polym. J. 167. https://doi.org/10.1016/j.eurpolymj.2022.111074.
Wever, D.A.Z., Picchioni, F., Broekhuis, A.A., 2011. Polymers for enhanced oil recovery: A paradigm for structure-property relationship in aqueous solution. Prog. Polym. Sci. 36 (11), 1558–1628. https://doi.org/10.1016/j.progpolymsci.2011.05.006.
Wu, Z., Li, H., Zhao, X., Ye, F., Zhao, G., 2022. Hydrophobically modified polysaccharides and their self-assembled systems: A review on structures and food applications. Carbohydr. Polym. 284. https://doi.org/10.1016/j.carbpol.2022.119182.
Xiang, W., Li, L., Dong, Y., Wang, Z., Song, Z., Zhao, M., Dai, C., 2025. Ultra-high temperature and salinity resistant microspheres featuring “Rigid hydrophobic core-soft hydrophilic Shell” structure for deep reservoir profile control. Chem. Eng. J. 509. https://doi.org/10.1016/j.cej.2025.161432.
Xu, L., Xu, G., Liu, T., Chen, Y., Gong, H., 2013. The comparison of rheological properties of aqueous welan gum and xanthan gum solutions. Carbohydr. Polym. 92 (1), 516–522. https://doi.org/10.1016/j.carbpol.2012.09.082.
Xu, L., Xu, G., Yu, L., Gong, H., Dong, M., Li, Y., 2014. The displacement efficiency and rheology of welan gum for enhanced heavy oil recovery. Polym. Adv. Technol. 25 (10), 1122–1129. https://doi.org/10.1002/pat.3364.
Zhang, H., Gou, S., Zhou, L., Fei, Y., Peng, C., Huang, J., Chen, L., 2019. Modified polyacrylamide containing phenylsulfonamide and betaine sulfonate with excellent viscoelasticity for EOR. J. Appl. Polym. Sci. 136 (38). https://doi.org/10.1002/app.47971.
Zhang, P., Wang, Y., Chen, W., Yu, H., Qi, Z., Li, K., 2011. Preparation and solution characteristics of a novel hydrophobically associating terpolymer for enhanced oil recovery. J. Solut. Chem. 40 (3), 447–457. https://doi.org/10.1007/s10953-011-9663-9.
Ziabakhsh-Ganji, Z., Nick, H.M., Donselaar, M.E., Bruhn, D.F., 2018. Synergy potential for oil and geothermal energy exploitation. Appl. Energy 212, 1433–1447. https://doi.org/10.1016/j.apenergy.2017.12.113.